Updating land cover map based on change detection of high-resolution remote sensing images

Rui Guo,[a] Pengfeng Xiao,[a,b,*] Xueliang Zhang,[a] and Hao Liu[a]
[a]Nanjing University, School of Geography and Ocean Science, Jiangsu Provincial Key Laboratory of Geographic Information Science and Technology, Key Laboratory for Land Satellite Remote Sensing Applications of Ministry of Natural Resources, Nanjing, China
[b]Jiangsu Center for Collaborative Innovation in Geographical Information Resource Development and Application, Nanjing, China

Abstract. Multi-temporal high-resolution land cover (LC) information is of great significance to landscape monitoring, environmental assessment, and local climate change. Given the LC map in the former phase, an automatic LC updating approach based on change detection of high-resolution remote sensing images is proposed. First, object-based change detection is implemented combining spectral bands, normalized difference vegetation index, and normalized difference water index. Second, the changed objects are classified using training samples generated from the unchanged area, and the LC labels of the training samples were transferred from the LC map in the former phase. Finally, as the updated objects with abnormal area (AREA) or perimeter-area ratio (PARA) are recognized as slivers or spurious stretches, and removed using specifically designed rules, an AREA-PARA-based updating method is proposed to update the LC map. Two pairs of GaoFen-1 panchromatic and multispectral sensor images acquired in 2013 and 2015 of two areas in Jiangsu, China, were used to validate the effectiveness of the proposed method. Results and the comparisons with two other updating methods manifested the superiority of the APU method in reducing abnormal LC fragmentation and shape complexity, and maintaining LC consistency between two phases. [DOI: 10.1117/1.JRS.15.044507]

Keywords: high-resolution remote sensing images; automatic land cover update; change detection; object-based.

Paper 210301 received May 8, 2021; accepted for publication Oct. 12, 2021; published online Oct. 28, 2021.

1 Introduction

Land cover (LC) and its changes significantly influence the Earth's biosphere, hydrosphere, and atmosphere.[1–4] Consequently, multi-temporal LC maps of various resolutions are increasingly required for numerous applications, such as natural resource management, biodiversity assessment, and environmental change monitoring.[4–8] Over the past 40 years, multi-temporal global LC products of diverse spatial resolutions have been produced using remote sensing images, such as MODIS yearly LC products at 500-m resolution,[9–11] CCI_LC dataset at 300-m resolution, GlobeLand30 at 30-m resolution,[12] and FROM-GLC dataset at 30-m resolution.[13,14] However, time series of accurate LC map with higher resolutions are still in urgent demand with the easy access of high-temporal and -spatial remote sensing images, e.g., Quickbird-1/2, WorkView-1/2/3, and GaoFen-1/2.[1,10,15–19]

Considerable efforts have been devoted to developing automatic LC updating methods. However, accurately LC updating is still challenging because of classification instability and inevitable human intervention.[1,6,12,15,20–25]

The updating method based on change detection serves as a promising solution, where classification task is restrained to only the changed area and therefore both the classification accuracy and consistency can be greatly improved.[2,3,17,26] Nevertheless, the updating accuracy depends on several aspects, e.g., change detection algorithms, LC labeling, and updating methods.

*Address all correspondence to Pengfeng Xiao, xiaopf@nju.edu.cn

1931-3195/2021/$28.00

Generally, change detection methods are categorized into two types: post-classification comparison and direct comparison.[3] Post-classification comparison methods determine LC changes by comparing the classifications in different phases, the challenge of which is to maintain the classification stability across multi-phases. Instead, direct comparison methods determine LC changes by analyzing the change magnitudes of image features, e.g., difference analysis, ratio analysis, and change vector analysis (CVA), thereby avoiding the introducing of classification errors.[3,26] Two issues need to be handled for direct comparison methods: one is to determine the indicators used to characterize the change magnitude, and the other is to clarify whether a given indicator exceeds a specific limit or threshold. Usually, to obtain high change detection accuracy, direct comparison methods have strict requirements for satellite sensor, image quality, and acquisition phenology of the images.[1–3]

In addition to the challenge of change detection, LC labeling for the changed area is another important issue for LC updating. When ground reference data are available, the process of LC updating can be particularly effective with a supervised approach.[16,27] However, gathering reliable ground reference data for each specific acquisition date is not realistic. Hence, researchers are applying transfer learning techniques (domain adaptation) to sample selection procedure,[16,27–31] where transfer learning are based on two assumptions: (1) the LC types in the source domain should be the same with those in the target domain; and (2) the statistical distributions of the LC in two phases should be sufficiently correlated.

An inevitable and severe issue occurring in the LC updating of the changed area is the boundary mismatch between the changed units and the unchanged units due to the segmentation discrepancy in different phases or the change detection error.[17,23,32] Generally, the LC map in the baseline is regarded as the Ref. 23. Specifically, slivers and spurious stretches are two forms of boundary mismatch. Slivers are the undershoots or under-detected parts between the change object and the adjacent baseline LC object, and spurious stretches are the overshoots or over-detected parts around the boundaries of the change object, both of which result in the abnormal LC fragmentation and shape complexity in the updated map.

Boundary mismatch can induce large bias in patch-based metrics, such as number of patches (NP), edge density (ED), landscape shape index (LSI), and mean of contiguity index (Contig_mn), thereby distorting the quantification of LC changes inferred from landscape pattern analyses.[33–35] Therefore, the recognition and processing of slivers and spurious stretches play important roles in the updating strategy, i.e., to distinguish real changes from slivers and spurious stretches. In many operational scenarios, researchers recognize a sliver using size-based parameter, e.g., minimum mapping width (MMW), minimum mapping unit (MMU), and area (AREA), or together with shape-based parameter such as perimeter-area ratio (PARA). The recognized sliver is then merged with its nearest object having the maximum area, or the longest shared border, or the same LC type.[23,32,33,36,37] On the other hand, little attention has been paid to spurious stretches. One study shed light on why slivers and spurious stretches come into existence, and offered a solution in a raster environment.[17] In this case, the changed area was manually delineated, and a sliver was merged with its nearest change object, and a spurious stretch was deleted from the change object, once they are recognized by MMW through boundary-matching. Moreover, it was suggested that the modification in the updating is limited to the scope of the changed area so that the unchanged baseline LC objects are not affected. However, this method has strict requirements for the accuracy of change detection. Furthermore, in the context of automatic updating, a certain proportion of sliver and spurious stretch tends to have relatively large size and complicated shape, which makes them difficult to be recognized using only area-based parameter. In view of this, the updating strategy to include both the size-based and the shape-based parameters for sliver and spurious stretch recognition is quite promising.

During automatic updating of LC maps, sliver and spurious stretch will emerge around the boundaries of the change objects and the neighboring baseline objects owing to the boundary mismatch. Some are characterized with small size, and the others with slender or more complicated shape. Though sliver and spurious stretch usually exert a small influence on the final updating accuracy, they can induce large bias in patch-based metrics and thus distort the quantification of LC changes inferred from landscape pattern analyses. According to their characteristics, it is hopeful to recognize them using the size- and shape-based parameters. Given the

urgent need for up-to-date LC maps with high-spatial resolutions, we aim to explore an automatic approach to update LC maps based on change detection using high-spatial resolution images. First, we take the direct comparison change detection strategy and determine the change thresholds automatically. Then, the changed area was labeled through supervised classification, and transfer learning is applied to sample selection. Finally, LC updating is carried out using AREA-PARA-based updating (APU) method on the basis of the baseline LC map.

The main contributions of this study are as follows: (1) we proposed the APU method for LC updating based on vector rules. The APU method can efficiently remove slivers and spurious stretches arising from boundary mismatch, and thus restrain abnormal LC fragmentation and shape complexity occurred in the map production; (2) we proved that the proposed approach can promote the LC consistency between different phases, since it puts much emphasis on inheriting both LC types and LC boundaries from the baseline LC map; and (3) we achieved accurate LC updating using high-resolution images in a typical suburban area (SA) and a representative urban area (UA).

2 Study Area and Data

Two study areas were selected to test the proposed updating approach. The focus area is a typical SA located at Nanjing, and the extended area is a typical UA located at Zhenjiang, both of which are in Jiangsu Province, China (Fig. 1). The study area SA covers an area of 4.2 km^2, and consists of natural LC (i.e., forest, shrub, grass, barren, and ponds) and artificial LC (i.e., buildings, roads, and reservoir). The study area UA covers an area of 22.1 km^2 and is dominated by artificial LC, including building, barren under construction, and road, while natural LC accounts for only a small portion, including green land and river.

GaoFen-1 (GF-1) Panchromatic and Multispectral Sensor (PMS) images with one 2-m resolution panchromatic band and four 8-m resolution multispectral bands were used in this study. Due to the limited access to GF-1 PMS images in the same month, images acquired on July 12, 2013, and May 22, 2015, were selected. These images can be roughly counted in the same phenological season because most vegetation have turn green in May in the study areas. In this study, the baseline is year 2013 (labeled as T1), and the target phase is year 2015 (labeled as T2).

Image pre-processing includes panchromatic sharpening in the individual phase, and geometric registration and relative radiometric calibration between the pan-sharpened images in two phases. Panchromatic sharpening was implemented using Gram–Schmidt method, the processed multispectral images having a spatial resolution of 2 m. Geometric registration was carried out using a polynomial function based on 60 ground control points, where the root mean square error (RMSE) is within 0.5 pixel. Relative radiometric calibration was conducted through histogram matching. As the terrain of the study areas has little variation, ortho-rectified correction was thus not conducted.

The pre-processed GF-1 images in the study areas are shown in Figs. 1(b), 1(c), and 1(e), 1(f). The LC is categorized into five types, i.e., vegetation, barren, water, road, and building, which are described in Table 1. The baseline LC maps for the two study areas were acquired by visual interpretation, as shown in Figs. 1(d) and 1(g). Considering the complexity of the surface features in the study area UA, some residential areas were delineated into a whole residential area instead of individual buildings and roads to release workload. It has been confirmed that these residential areas stayed unchanged during T1 and T2.

3 Methodology

3.1 *Overview*

The framework of the proposed approach is shown in Fig. 2. First, the pre-processed GF-1 PMS images in T1 and T2 were compared through difference operation to derive the changed area using the selected image features. Second, LC labeling for the changed area was accomplished by supervised classification using the training samples selected from the unchanged area in the image of T2, and the LC labels are transferred from the LC map in T1. Finally, the labeled

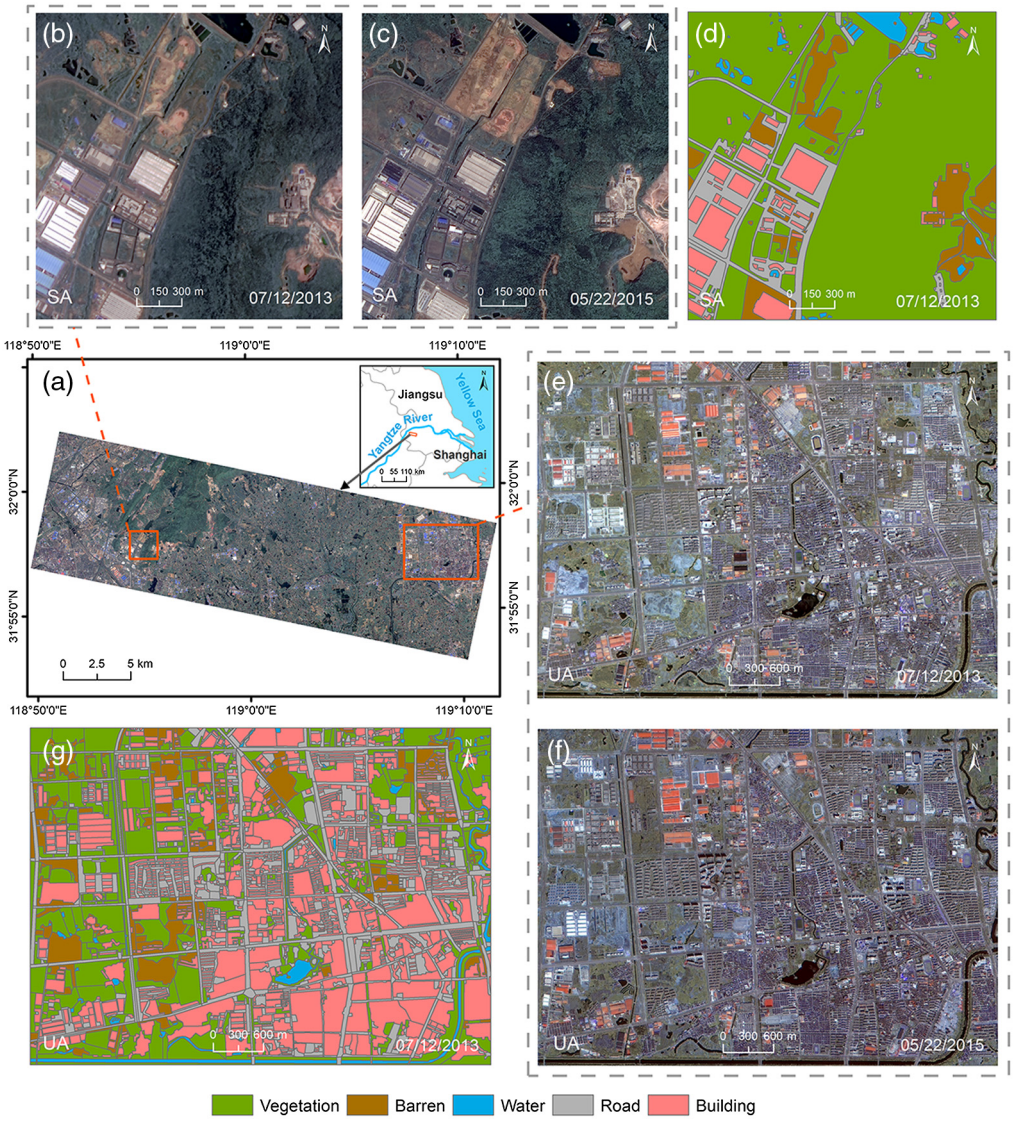

Fig. 1 Illustration of the two study areas and data. The images in the two study areas are taken from the overlapping area of the pre-processed GF-1 PMS images acquired on July 12, 2013, and May 22, 2015. (b) and (c) The images in the SA, and (e) and (f) the images in UA, both with true-color composite (Red: band 3, Green: band 2, Blue: band 1). (d) and (g) The reference LC maps in 2013 of the study area SA and UA, respectively.

Table 1 LC types and descriptions in the two study areas.

ID	Type	Description
1	Vegetation	Forest, shrub, and grassland
2	Barren	Open land under construction or without vegetation
3	Water	River, lake, reservoir, and pond
4	Road	Natural road, square, tarred road, cement road, pavement, and playground
5	Building	Building in use, and building newly built

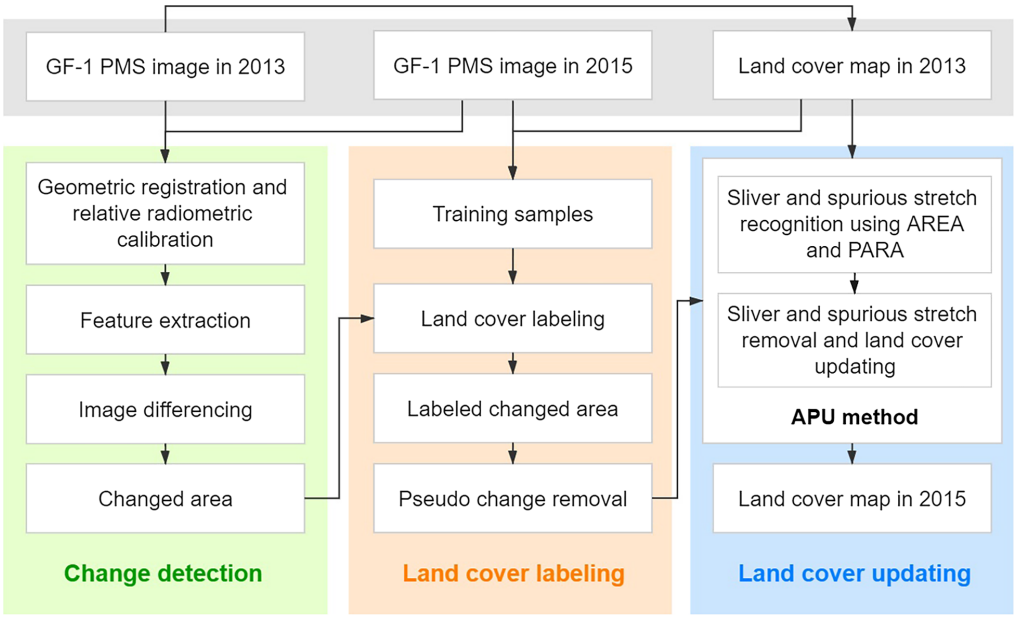

Fig. 2 Framework of the proposed LC updating approach.

change objects were processed to remove pseudo changes, and then used to update the changed objects in the LC map of T1 by the APU method to obtain the LC map in T2.

3.2 *Change Detection*

We took direct comparison strategy and conducted object-based change detection to acquire change objects in T2 for the sake of simplicity and efficiency. Multi-temporal image segmentation strategy was adopted first, where a stack of spectral bands in two phases were segmented together to make sure the objects in the two phases have the same geometric properties.[38] The multi-resolution segmentation algorithm[39] was used to derive homogeneous objects from the images, and the average value of the pixels in the object was used as the feature value of the object. The segmentation parameters included shape, compactness, and scale. The scale parameter was determined by trial-and-error strategy to make sure the images are over-segmented at a certain extent, so that change under-detection can be reduced.

Many studies suggested that the combination of spectral bands and indexes can effectively capture the change information.[36,40] Thus, the four multispectral bands, normalized difference vegetation index (NDVI), and normalized difference water index (NDWI) were selected as the image features. CVA is a simple and effective method to detect multiple types of change through spectral vectors. The final change detection result was the union of the changes detected by CVA, NDVI, and NDWI. On the one hand, the area where the change magnitude of CVA exceeded the corresponding threshold was recognized as actual changes. On the other hand, the changes of NDVI and NDWI were achieved by difference operation, but only those area where the difference values exceeded the corresponding thresholds would be recognized as actual changes. Assuming a pixel's values in two images T1 and T2 are represented by vector $R = (r_1, r_2, \cdots, r_n)^{\mathrm{T}}$ and $S = (s_1, s_2, \cdots, s_n)^{\mathrm{T}}$, respectively, where n is the number of bands, a change vector Δ in CVA can be defined as[26]

$$\Delta = R - S = \begin{pmatrix} r_1 - s_1 \\ r_2 - s_2 \\ \vdots \\ r_n - s_n \end{pmatrix}. \tag{1}$$

The change magnitude $\|\Delta\|$ of the pixel is defined as[26]

$$\|\Delta\| = \sqrt{(r_1 - s_1)^2 + (r_2 - s_2)^2 + \cdots + (r_n - s_n)^2}. \quad (2)$$

The higher the change magnitude is, the greater the probability of the change is.

The Otsu algorithm[41] was applied to selecting the change threshold automatically for each change indicator, because it is simple, parameter free, and has proved efficient for change threshold selection.[42] To ensure that the selected thresholds were optimal, we further adopted trial-and-error strategy to make appropriate corrections to the thresholds. In this study, we aimed to determine a single threshold for multiple LC change types in CVA to improve efficiency.

In the two study areas, we randomly selected 200 validation pixels which were distributed proportionally to the area covered by each LC type to evaluate the accuracy of change detection and LC updating. The change condition and LC type of these validation pixels were determined by visually interpreting GF-1 images and were confirmed on Google Earth. The evaluation measures include overall accuracy (OA), Kappa coefficient (Kappa), user's accuracy, and producer's accuracy.

3.3 *Land Cover Labeling*

LC types of the change objects in T2 were labeled by the K-nearest neighbor classifier due to its simplicity and flexibility.[43,44] Since there were no LC types disappearing or new LC types appearing in T2, the training samples were selected from the unchanged area in T2, with the LC labels transferred from the LC map in T1. The feature space including spectral bands, NDVI, and NDWI was optimized by the class separation distance and participated in classification. The best class separation distance is the biggest distance of the closest classes calculated in the feature space of various dimensions, in which case the optimal feature set was achieved. The optimized feature set includes NDVI, NDWI, band 1, band 3, and band 4.

Since under-detection and over-detection tend to generate slivers and spurious stretches, it is suggested that the pseudo changes are removed after LC labeling and before LC updating. Two rounds of pseudo change removal were carried out: (1) when LC labeling for the change objects is finished, compare the classification result of the changed area with the corresponding LC types in the baseline map, and remove the pixels from the changed area whose LC types have not changed, which are viewed as pseudo changes; and (2) the remaining change objects whose AREA is smaller or PARA greater than the corresponding threshold would be recognized as meaningless and removed.

3.4 *Land Cover Updating*

During LC updating, slivers and spurious stretches can be generated due to boundary inconsistency of the change objects and the baseline objects, which arises from segmentation discrepancy in different phases and change detection error. The key to dealing with them is to recognize them according to their characteristics and then take different strategies. Linke et al.[17] proposed a method based on the size-based parameter MMW to recognize slivers and spurious stretches through boundary-matching for the raster data. After recognizing the sliver and spurious stretch, they merged the sliver with its nearest change object, and deleted the spurious stretch from the change object. This method did help to remove those slivers and spurious stretches having regular shape and small size, but it cannot remove the slivers with complicated shape and big size, which account for a certain proportion. In this condition, it is worth trying the shape-based parameter such as PARA for sliver and spurious stretch recognition.

From this perspective, the APU method is proposed in this study: (1) it uses both AREA and PARA of the change objects for sliver and spurious stretch recognition; and (2) sliver and spurious stretch are removed and the LC of the changed area are updated using vector rules. Especially, this updating scheme is designed for vector data so as to take advantage of its superiority in geometric calculation and easy access of topology relationships among the LC objects.

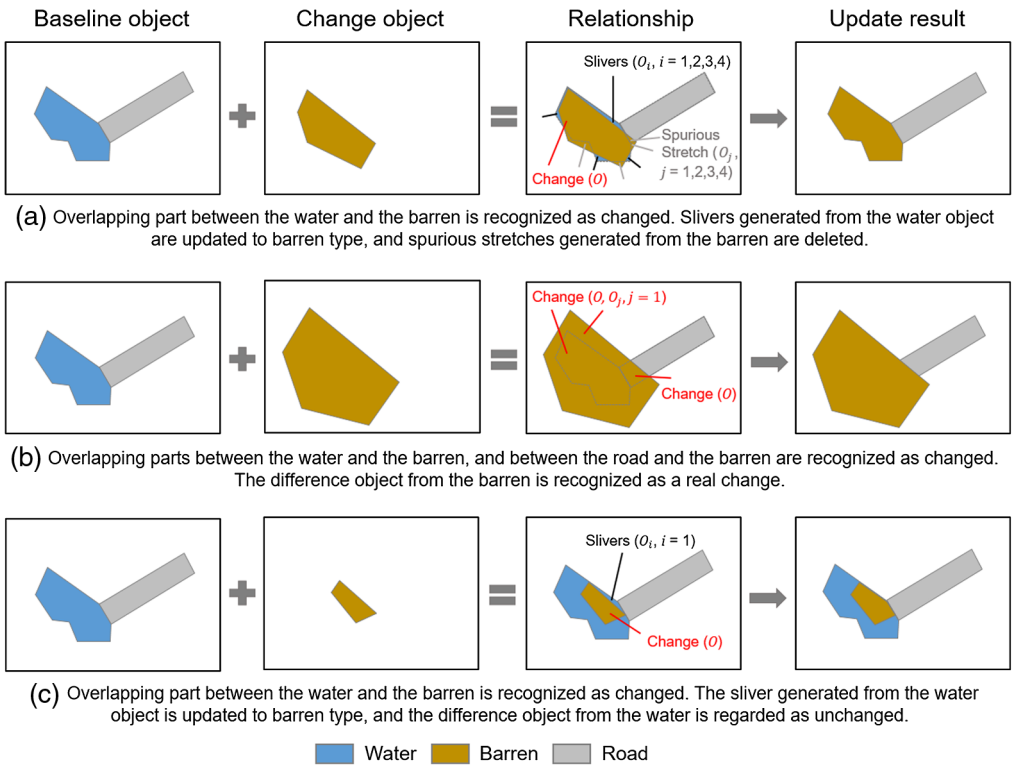

Fig. 3 Diagram describing the LC updating process using the APU method.

Step 1: sliver and spurious stretch recognition

Perform relationship operations to the change object and the baseline object, and judge if the generated objects during the operation are slivers or spurious stretches. The objects to be judged include the object as their common part (intersection operation result) and the objects as their individual different parts (difference operation result). The criterion to judge whether an object is a sliver or a spurious stretch is that the AREA of the object is smaller than AREA threshold or the PARA is greater than PARA threshold. If an object is a sliver or a spurious stretch, go to Step 2; otherwise, retain the object if it is the difference operation result, and retain the object belonging to the change object while deleting the corresponding one from the baseline object if it is the intersection operation result.

Step 2: sliver and spurious stretch removal and LC updating

If the object is a sliver, update its LC type with that of the change object; if the object is a spurious stretch, delete it. A diagram describing the updating process using the APU method is shown in Fig. 3. $O_i(i = 1, 2, 3\ldots)$ is the object in the difference result of the baseline object with the change object; $O_j(j = 1, 2, 3\ldots)$ is the object in the difference result of the change object with the baseline object; O represents the overlapping part in the change object.

It is noted that AREA threshold cannot exceed the area of the smallest LC object in T1 and T2, and PARA threshold cannot be smaller than the PARA value of the most complex LC object in T1 and T2. In this study, we selected the area of the smallest LC object in T1 and T2 as AREA threshold, and selected the PARA value of the most complex LC object in T1 and T2 as PARA threshold. Both AREA and PARA threshold are consistent in the pseudo change removal procedure and the LC updating procedure. The whole algorithm was implemented with the help of the Shapely Python package.

It was demonstrated that slivers and spurious stretches have the potential to severely alter landscape patterns, thus we chose some landscape metrics related to fragmentation and shape complexity to evaluate the effectiveness of the APU method, which were NP, ED, LSI, and Contig_mn. These landscape metrics were calculated in Fragstats.

To evaluate the superiority of the APU method in reducing LC fragmentation while updating LC information, two other popular methods were designed and carried out in the two study areas. One is aimed at removing only slivers using AREA and PARA while updating LC change objects, and the other is aimed at removing both slivers and spurious stretches using only AREA while updating LC change objects (named AU method). We carried out the former method by combining overlay operation and "eliminate" tool provided by ArcMap (named COE method), in which slivers were recognized by AREA and PARA attributes, and merged with its nearest object having the largest area or the longest shared border. To carry out AU method, we made some modification on the basis of the APU method. Specifically, in our experiments using the COE method, slivers were merged with the nearest object having the longest shared border because this brought better results than being merged with the nearest object having the maximum area.

4 Results

4.1 *Accuracy of Change Detection*

The final change detection results in the study area SA and UA are shown in Fig. 4. The segmentation parameters are shown in Table 2, and the thresholds during LC updating are shown in Table 3. The accuracy at different change detection stages is shown in Tables 4 and 5, including the accuracy of the original change detection result (original), the accuracy of the change

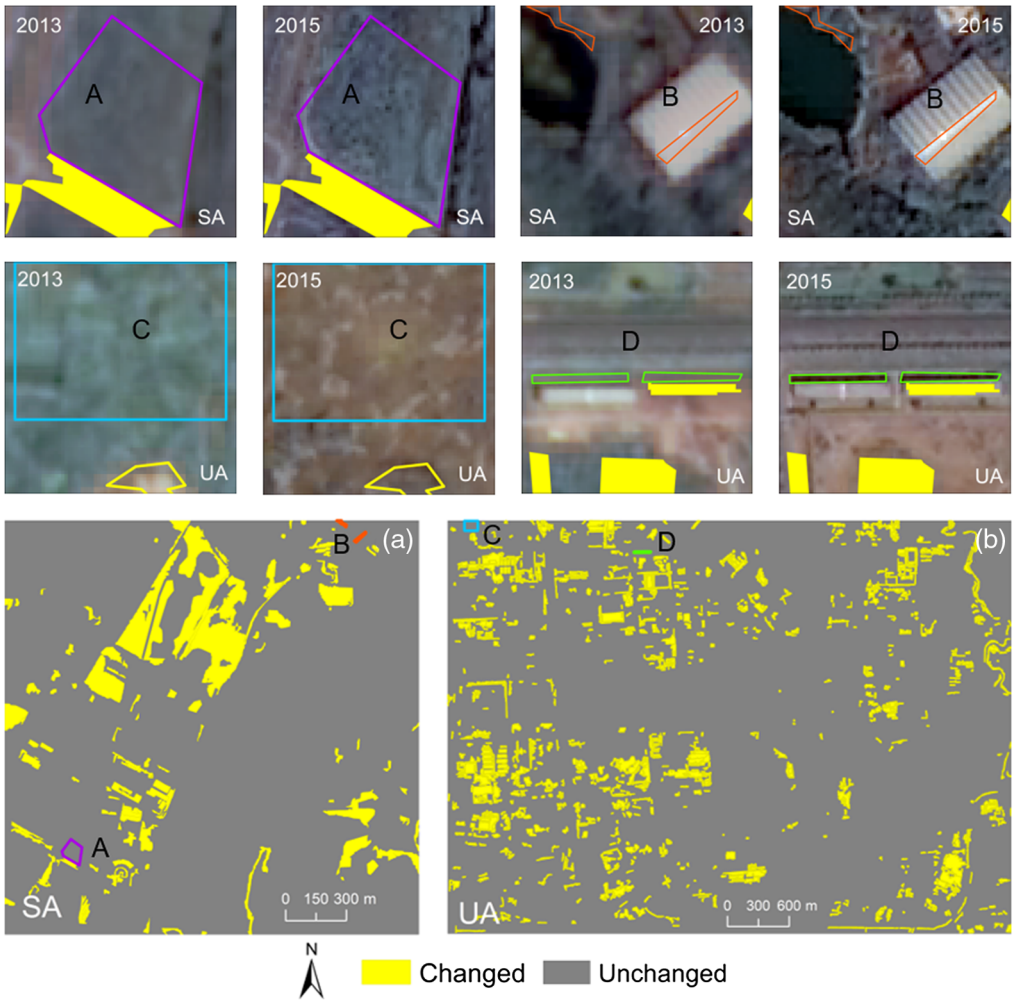

Fig. 4 Final change detection result in the study area (a) SA and (b) UA.

Table 2 Segmentation parameters of the two study areas.

Study area	Shape	Compactness	Scale
SA	0.1	0.5	40
UA	0.1	0.5	50

Table 3 Thresholds during LC updating in the two study areas.

Study area	Change magnitude in CVA	Change of NDVI	Change of NDWI	AREA	PARA
SA	97	0.14	0.10	80	0.404
UA	174	0.19	0.16	90	0.416

Table 4 Change detection accuracy at different stages in the study area SA.

		Reference			
Stage	Result	Unchanged	Changed	Sum	User's accuracy (%)
Original	Unchanged	157	3	160	98.12
	Changed	24	16	40	40.00
	Sum	181	19	200	—
	Producer's accuracy (%)	86.74	84.21	—	—
		OA: 86.5% Kappa: 0.47			
Labeled	Unchanged	177	3	180	98.33
	Changed	4	16	20	80.00
—	Sum	181	19	200	—
	Producer's accuracy (%)	97.79	84.21	—	—
		OA: 96.5% Kappa: 0.80			
AREA-PARA	Unchanged	177	3	180	98.33
	Changed	4	16	20	80.00
	Sum	181	19	200	—
	Producer's accuracy (%)	97.79	84.21	—	—
		OA: 96.5% Kappa: 0.80			

detection result refined by comparing the LC labels with those in T1 (labeled), and the accuracy of the change detection result refined with AREA and PARA (AREA-PARA).

In the study area SA, OA had an increase of 10% points, and Kappa coefficient improved by 0.33, and the user's accuracy of the changed area had an increase of 40% points, after the original change detection result being refined with the LC labels of the change objects. It indicates that the consideration of both spectral change and label change can help to detect the real changes (e.g., the pseudo vegetation change marked by the purple polygon in Fig. 4 was detected and removed after being correctly classified).

Table 5 Change detection accuracy at different stages in the study area UA.

Stage	Result	Reference			
		Unchanged	Changed	Sum	User's accuracy (%)
Original	Unchanged	141	6	147	95.92
	Changed	19	34	53	64.15
	Sum	160	40	200	—
	Producer's accuracy (%)	88.13	85.00	—	—
		OA: 87.5% Kappa: 0.65			
Labeled	Unchanged	156	18	174	89.66
	Changed	4	22	26	84.62
	Sum	160	40	200	—
	Producer's accuracy (%)	97.50	55.00	—	—
		OA: 89.0% Kappa: 0.60			
AREA-PARA	Unchanged	156	18	174	89.66
	Changed	4	22	26	84.62
	Sum	160	40	200	—
	Producer's accuracy (%)	97.50	55.00	—	—
		OA: 89.0% Kappa: 0.60			

In the study area UA, OA had an increase of 1.5% points, and the user's accuracy of the changed area had an increase of 20.47% points after the original change detection result being refined with the LC labels of the change objects, while Kappa coefficient had a tiny decrease. The producer's accuracy of the changed area had a certain decrease, because labeling errors led to some real changes being removed (e.g., the detected real vegetation change to barren in the extent marked by the blue rectangle in Fig. 4 was falsely labeled as vegetation and removed due to the spectral interference of the sparse grass). Compared with the study area SA, the surface features in the study area UA are more complex and the patch size of multiple LC types is smaller, both of which make it more challenging to achieve high accuracy in change detection and LC labeling of the changed area.

AREA and PARA brought evident improvements to the change detection result, e.g., the pseudo changes marked by the red and green polygons in Fig. 4 were detected and removed at AREA-PARA stage. However, these improvements failed to be reflected in the validation results because both the proportion and the patch size of the fragmented pseudo changes were very small, and the probability for the validation points to be distributed there is low.

Furthermore, comparing the change detection results of the two study areas, we found that CVA of bands is capable of capturing most changes, especially for the change of artificial LC types, while NDVI and NDWI are still important for detecting changes of vegetation and water. Moreover, Otsu algorithm is automatic and simple to select change thresholds, while trial-and-error strategy is flexible. The combination of the two is suitable to obtain the optimal change thresholds.

4.2 *Accuracy of Land Cover Updating*

The GF-1 images in T2 and the updated results in the two study areas are shown in Fig. 5 and 6, and the confusion matrices are shown in Tables 6 and 7. Relatively high LC updating accuracy

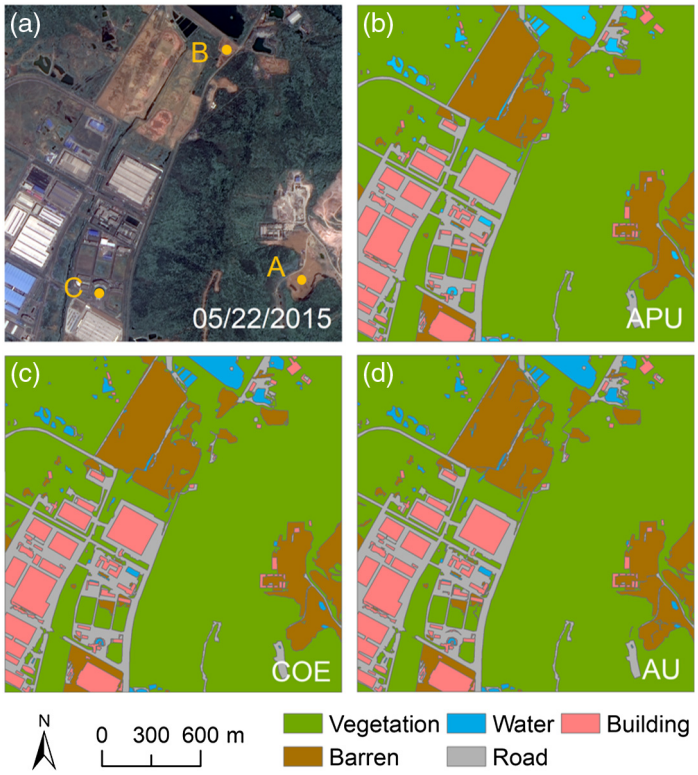

Fig. 5 Comparison of (a) the GF-1 image in 2015 and the updated LC map using the (b) APU, (c) COE, and (d) AU method in the study area SA. The details of location A, B, and C are shown in Fig. 7.

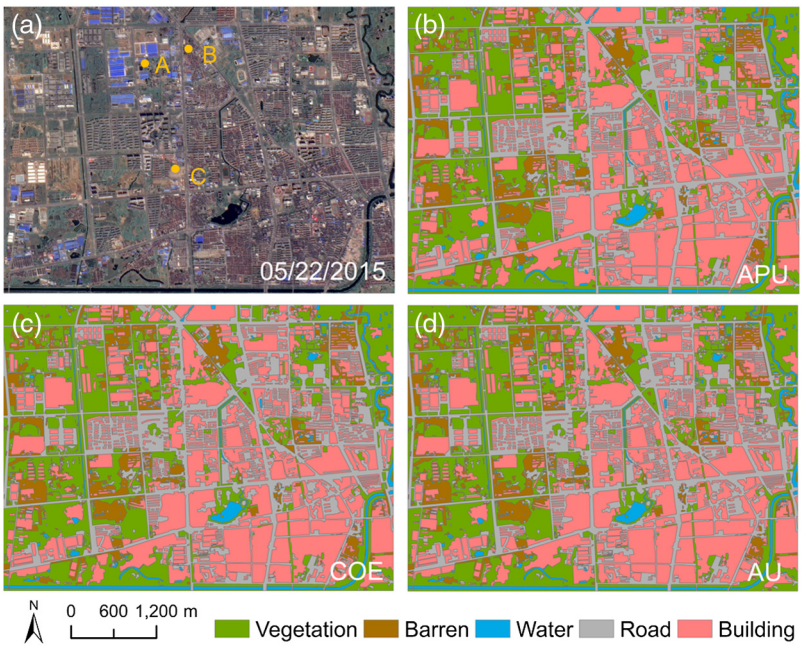

Fig. 6 Comparison of (a) the GF-1 image in 2015 and the updated LC map using the (b) APU, (c) COE, and (d) AU method in the study area UA. The details of location A, B, and C are shown in Fig. 8.

Table 6 Confusion matrix of the updated LC map in 2015 using the APU method in the study area SA.

	Reference					
Result	Vegetation	Barren	Water	Road	Building	User's accuracy (%)
Vegetation	117	5	0	3	0	94
Barren	0	29	0	1	0	97
Water	0	0	7	0	0	100
Road	0	1	0	22	0	96
Building	0	0	0	0	15	100
Producer's accuracy (%)	100	83	100	85	100	—
OA: 95%, Kappa: 0.91						

Table 7 Confusion matrix of the updated LC map in 2015 using the APU method in the study area UA.

	Reference					
Result	Vegetation	Barren	Water	Road	Building	User's accuracy (%)
Vegetation	37	5	0	0	2	84
Barren	5	12	0	1	1	63
Water	1	0	9	1	0	82
Road	1	5	0	26	8	65
Building	0	1	1	3	81	94
Producer's accuracy (%)	84	52	90	84	88	—
OA: 83%, Kappa: 0.75						

was achieved, with OA and Kappa 95% and 0.91 in the study area SA, and 83% and 0.75 in the study area UA. Labeling errors mainly occurred in barren and road due to spectral similarity. In some cases, roofs were made from the same material with the roads, e.g., cement and asphalt, and natural roads may have similar spectrums with barren. Sparse grass or shrubs are important factors affecting the classification accuracy of vegetation and barren. The main change types in the two study areas during T1–T2 are "vegetation change from/to barren," barren change from/to building/road, and vegetation change from/to building/road owing to urban expansion and reconstruction.

According to the landscape metrics results in Table 8, both the number and the shape complexity of LC objects underwent certain rises during the period of T1–T2 in the two study areas. Furthermore, the selected landscape metrics indicate that the LC is more diverse and complex in the study area UA than SA, which conforms to the actual situation.

Statistics show that slivers and spurious stretches processed in the updating process account for only 0.255 % for the study area SA, and 0.091% for the study area UA, too small to cause numerical differences on OA. As the threshold for AREA cannot be greater and the threshold for PARA cannot be smaller than the thresholds we already selected, to avoid that a real change is falsely removed, we conclude that AREA and PARA are not sensitive to OA of the updating results. Even so, it is still suggested to select a big threshold for AREA within the range of the

Table 8 Landscape metrics results in the two study areas in T1 and T2.

Study area	Image	Landscape metrics			
		Number of patches	Edge density	Landscape shape index	Mean of contiguity index
Suburban area	T1	184	169.63	9.68	0.86
	T2	286	189.04	10.68	0.70
Urban area	T1	1303	270.10	32.73	0.93
	T2	2254	325.63	39.24	0.80

smallest LC object in T1 and T2, and to select a small threshold for PARA beyond the maximum value of PARA for LC objects in T1 and T2, because that will better reduce abnormal LC fragmentation in T2 without affecting the updating accuracy.

4.3 *Comparison with Other Methods*

The updating results using the COE and the AU methods in the study area SA are presented in Figs. 5(c) and 5(d), and the details at location A, B, and C are shown in Fig. 7. At location A, some slivers whose area exceeds AREA threshold still remained in the result of AU method, while were removed in the results of the other two methods. Moreover, part of one road was wrongly updated by an object that was mistakenly detected as changed and falsely labeled as vegetation in the results of the COE and the AU methods, but was successfully retained in the result of the APU method owing to the recognition of spurious vegetation stretch using PARA. At location B, the barren was over-detected at its border with the road. Both the COE and the AU methods took this over-detected part as real change, while the APU method recognized it as spurious barren stretch using PARA and deleted it from the barren. The shared border and this part of road were thus preserved. At location C, part of the water object near its boundaries was detected as changed falsely, and was further misclassified as building. In the result of the COE

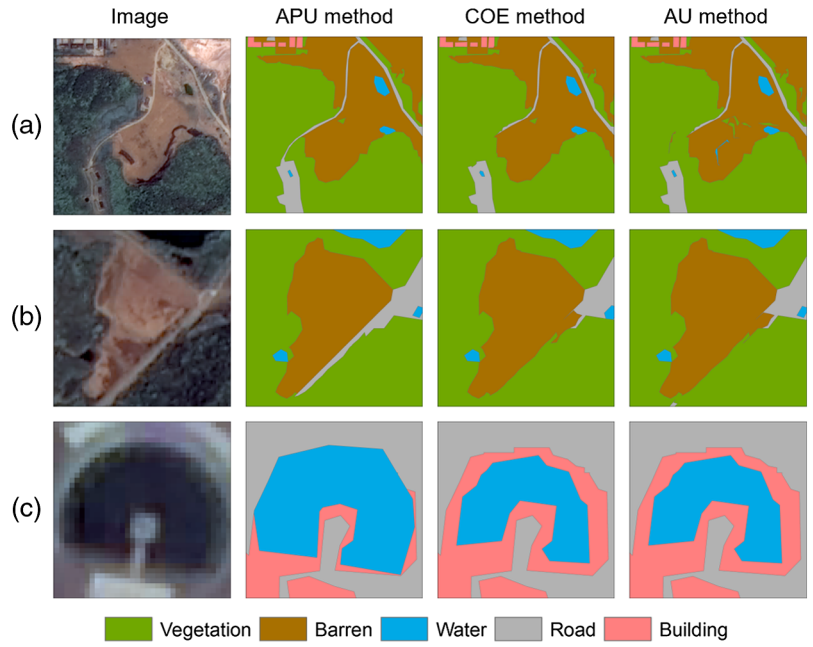

Fig. 7 Comparison of the GF-1 image in 2015, the updating results using the APU, COE, and AU method at location A, B, and C in the study area SA.

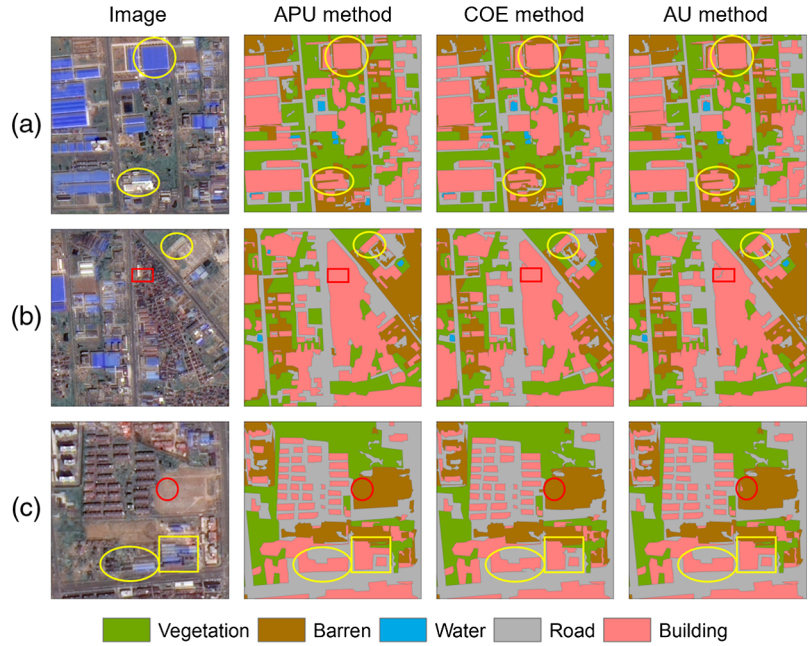

Fig. 8 Comparison of the GF-1 image in 2015, the updating results using the APU, COE, and AU method at location A, B, and C in the study area UA. The yellow marks show the cases where spurious stretches at the boundaries of the LC objects persisted in the result of the COE method, but were merged with the neighboring objects in the result of the APU method. The red marks show the cases where some slivers persisted in the result of AU method but were merged with the neighboring objects in the result of the APU method.

and the AU methods, the water appeared shrunk due to change detection and classification errors. But this pseudo change was successfully recognized as spurious building stretch using AREA and PARA, and was removed. In this way, the shape of this water object was preserved.

The updating results using the COE and the AU methods in the study area UA are presented in Figs. 6(c) and 6(d), and the details at location A, B, and C are shown in Fig. 8. In comparison, the boundaries of the LC objects in the result of the COE method tend to be encroached by spurious stretches (shown in the yellow marks), and the LC in the result of AU method appear more fragmented due to the persistence of some slivers (shown in the red marks). It can be seen from Fig. 8 that some slivers that were mistakenly detected as changed due to the spectral similarity between different LC types and further wrongly labeled were successfully recognized and merged with the neighboring objects in the result of the APU method (shown in the red marks). Besides, some spurious road and barren stretches encroaching the building were recognized and merged with the neighboring building in the result of the APU method, and the objects free of spurious stretches thus can retain their original boundaries in T1 (shown in the yellow marks).

OA and Kappa are the same for the results using the three methods in the two study areas. The comparison of landscape metrics derived from the updated results of the three methods in the study area SA and UA is shown in Table 9. Since we have delineated the reference LC maps in T1 for the two study areas, we assumed that the landscape metrics calculated from these reference maps are 'correct' values for T1. Besides, the correct metric values for T1 also served as the guideline for T2 to some extent, because the change of landscape pattern in T2 were certain but not dramatic according to the GF-1 images. As slivers and spurious stretches tend to increase fragmentation and shape complexity of LC, the smaller the change ranges of the landscape metrics between T1 and T2, the closer the results are to the 'correct' metric values for T2. Combining Tables 8 and 9, we can see that the APU method brought greater improvements in restraining abnormal LC fragmentation and shape complexity in the map production, and this is especially obvious in the study area SA. A possible explanation is that the segmentation scale for the study area SA is smaller than that for the study area UA, which results in more slivers and spurious stretches being generated and removed in the updating process.

Table 9 Landscape metrics results of the APU, COE, and AU method in the two study areas.

Study area	Updating method	Landscape metrics			
		Number of patches	Edge density	Landscape shape index	Mean of contiguity index
Suburban area	APU	286	189.04	10.68	0.70
	COE	314	191.28	10.80	0.65
	AU	479	203.23	11.41	0.53
Urban area	APU	2254	325.63	39.24	0.80
	COE	2366	333.77	40.20	0.79
	AU	2438	332.30	40.05	0.77

To conclude, the result of the APU method tends to inherit the boundaries from T1, during which spurious stretches can be recognized and removed by PARA, compared with the results of the AU and the COE methods. Furthermore, the APU method can greatly reduce abnormal LC fragmentation and shape complexity occurred in the map production, since more slivers can be recognized using both AREA and PARA. One limitation is that if the detected change object is a little smaller than the corresponding baseline object and then wrongly labeled, this mistake will be enlarged with the difference part of the change object and the baseline object being assigned the same false label. However, considering the tiny proportion of spurious stretches to the whole study area, this negative effect can be overlooked.

5 Discussion

According to the proposed updating process, the final accuracy mainly relies on four aspects: the baseline LC map, change detecting, LC labeling for the change objects, and LC updating using the change objects.

The baseline LC map mainly affects the final updating accuracy in two ways: (1) the labels in the unchanged area of T1 participate in the LC labeling of the change objects in T2 through sample selection procedure; and (2) the unchanged LC objects and part of the boundaries of the changed LC objects in T1 will persist in the updated LC map in T2. Therefore, an accurate baseline LC map is of high significance.

Change detection determines the area to be updated, while LC labeling decides whether the changed area will be correctly updated in the end. Besides, the accuracy of change detection will also affect the accuracy of LC labeling. If the real changes that were falsely recognized as unchanged were selected as training samples, the risk of misclassification will increase. Thus a certain percent of change over-detection is necessary. Furthermore, if these over-detected pseudo changes are correctly labeled, they will be removed from the change map in the pseudo change removal procedure, and OA for change detection will be improved. Meanwhile, with the extent of change over-detection enlarging, less candidate samples were left in the unchanged area for LC labeling, thus striking a balance between change over-detection and sample space is of great importance.

Over-detection and under-detection of change are inevitable for automatic change detection, and the boundary mismatch problem between the change object and the baseline object arising from segmentation and change detection errors need to be solved or restrained in the LC updating process. Though the proportion of the boundary mismatches in the updated LC map is very small by statistics, they have significant effects on the landscape patterns. The APU method uses AREA and PARA to recognize both slivers and spurious stretches, further reducing the requirement for change detection accuracy, and proves effective and superior in alleviating abnormal LC fragmentation occurred in the map production and retaining the boundaries of the baseline LC objects.

6 Conclusion

The study proposed a novel automatic LC updating approach using high-resolution images based on change detection. Applying this approach to a typical SA and an UA, we found that the APU method, which is based on vector rules can efficiently remove slivers and spurious stretches generated from the segmentation discrepancy in different phases or the change detection error, and thus restrain abnormal LC fragmentation and shape complexity in the updated map. It proved that the updated maps are capable of inheriting the unchanged objects and part of the boundaries of the changed objects from the baseline LC map, thus LC consistency between different phases was greatly promoted.

Acknowledgements

This work was supported by the National Natural Science Foundation of China under Grant Nos. 41871235 and 42071297. Disclosures: There is no relevant financial interests or other potential conflicts of interest in the manuscript.

References

1. X. Chen et al., "An improved automated land cover updating approach by integrating with downscaled NDVI time series data," *Remote Sens. Lett.* **6**(1), 29–38 (2015).
2. X. Chen et al., "An automated approach for updating land cover maps based on integrated change detection and classification methods," *ISPRS J. Photogramm, Remote Sens*, **71**, 86–95 (2012).
3. Y. Hu, Y. Dong, and Batunacun, "An automatic approach for land-change detection and land updates based on integrated NDVI timing analysis and the CVAPS method with GEE support," *ISPRS J. Photogramm. Remote Sens.* **146**, 347–359 (2018).
4. Z. Zhu and C. E. Woodcock, "Continuous change detection and classification of land cover using all available Landsat data," *Remote Sens. Environ.* **144**, 152–171 (2014).
5. P. Gong, X. Li, and W. Zhang, "40-year (1978–2017) human settlement changes in China reflected by impervious surfaces from satellite remote sensing," *Sci. Bull.* **64**(11), 756–763 (2019).
6. S. Jin et al., "A land cover change detection and classification protocol for updating Alaska NLCD 2001 to 2011," *Remote Sens. Environ.* **195**, 44–55 (2017).
7. R. Latifovic and D. Pouliot, "Multitemporal land cover mapping for Canada: methodology and products," *Can. J. Remote Sens.* **31**(5), 347–363 (2005).
8. H. Li et al., "Using land long-term data records to map land cover changes in China over 1981–2010," *IEEE J. Sel. Top. Appl. Earth Obs. Remote Sens*. **10**(4), 1372–1389 (2017).
9. M. A. Friedl et al., "MODIS Collection 5 global land cover: algorithm refinements and characterization of new datasets," *Remote Sens. Environ.* **114**(1), 168–182 (2010).
10. D. Sulla-Menashe et al., "Hierarchical mapping of annual global land cover 2001 to present: the MODIS Collection 6 land cover product," *Remote Sens. Environ.* **222**, 183–194 (2019).
11. D. Sulla-Menashe and M. A. Friedl, "User guide to Collection 6 MODIS land cover (MCD12Q1 and MCD12C1) product," (2018).
12. J. Chen et al., "Global land cover mapping at 30 m resolution: a POK-based operational approach," *ISPRS J. Photogramm. Remote Sens.* **103**, 7–27 (2015).
13. P. Gong et al., "Mapping essential urban land use categories in China (EULUC-China): preliminary results for 2018," *Sci. Bull.* **65**(3), 182–187 (2020).
14. P. Gong et al., "Finer resolution observation and monitoring of global land cover: first mapping results with Landsat TM and ETM+ data," *Int. J. Remote Sens.* **34**(7), 2607–2654 (2013).
15. J. A. Cardille and J. A. Fortin, "Bayesian updating of land-cover estimates in a data-rich environment," *Remote Sens. Environ.* **186**, 234–249 (2016).

16. S. Huang et al., "Updating land cover automatically based on change detection using satellite images: case study of national forests in Southern California," *GISci. Remote Sens.* **54**(4), 495–514 (2017).
17. J. Linke et al., "A disturbance-inventory framework for flexible and reliable landscape monitoring," *Photogramm. Eng. Remote Sens.* **75**(8), 981–995 (2009).
18. Y. Yang et al., "Accuracy assessment of seven global land cover datasets over China," *ISPRS J. Photogramm. Remote Sens.* **125**, 156–173 (2017).
19. Y. Zhao et al., "Detailed dynamic land cover mapping of Chile: accuracy improvement by integrating multi-temporal data," *Remote Sens. Environ.* **183**, 170–185 (2016).
20. A. Gressin et al., "A unified framework for land-cover database update and enrichment using satellite imagery," in *IEEE Int. Conf. Image Process.*, pp. 5057–5061 (2014).
21. J. Gong et al., "A review of multi-temporal remote sensing data change detection algorithms," *Remote Sens. Spatial Inf. Sci.* **37**, 757–762 (2008).
22. L. Ma et al., "Deep learning in remote sensing applications: a meta-analysis and review," *ISPRS J. Photogramm. Remote Sens.* **152**, 166–177 (2019).
23. G.J. McDermid et al., "Object-based approaches to change analysis and thematic map update: challenges and limitations," *Can. J. Remote Sens.* **34**(5), 462–466 (2008).
24. C. Paris, L. Bruzzone, and D. Fernández-Prieto, "A novel automatic approach to the update of land-cover maps by unsupervised classification of remote sensing images," in *IEEE Int. Geosci. Remote Sens. Symp.*, pp. 2207–2210 (2017).
25. X.-Y. Tong et al., "Land-cover classification with high-resolution remote sensing images using transferable deep models," *Remote Sens. Environ.* **237**, 111322 (2020).
26. G. Xian, C. Homer, and J. Fry, "Updating the 2001 National Land Cover Database land cover classification to 2006 by using Landsat imagery change detection methods," *Remote Sens. Environ.* **113**(6), 1133–1147 (2009).
27. L. Bruzzone and M. Marconcini, "Toward the automatic updating of land-cover maps by a domain-adaptation SVM classifier and a circular validation strategy," *IEEE Trans. Geosci. Remote Sens.* **47**(4), 1108–1122 (2009).
28. K. Bahirat et al., "A novel domain adaptation Bayesian classifier for updating land-cover maps with class differences in source and target domains," *IEEE Trans. Geosci. Remote Sens.* **50**(7), 2810–2826 (2012).
29. B. Demir, F. Bovolo, and L. Bruzzone, "Updating land-cover maps by classification of image time series: a novel change-detection-driven transfer learning approach," *IEEE Trans. Geosci. Remote Sens.* **51**(1), 300–312 (2013).
30. L. Shao, F. Zhu, and X. Li, "Transfer learning for visual categorization: a survey," *IEEE Trans. Neural Networks Learn. Syst.* **26**(5), 1019–1034 (2015).
31. Z. Wang et al., "A scale self-adapting segmentation approach and knowledge transfer for automatically updating land use/cover change databases using high spatial resolution images," *Int. J. Appl. Earth Obs. Geoinf.* **69**, 88–98 (2018).
32. L. Zhu, X. Wei, and R. Shi, "Fragment polygon removal in incremental land cover map updating," in *IGARSS IEEE Int. Geosci. and Remote Sens. Symp.*, IEEE, Yokohama, pp. 6511–6514 (2019).
33. J. Linke et al., "The influence of patch-delineation mismatches on multi-temporal landscape pattern analysis," *Landsc. Ecol.* **24**(2), 157–170 (2009).
34. G. Shao and J. Wu, "On the accuracy of landscape pattern analysis using remote sensing data," *Landsc. Ecol.* **23**(5), 505–511 (2008).
35. J. LaGro, Jr., "Assessing patch shape in landscape mosaics," *Photogramm. Eng. Remote Sens.* **57**(3), 285–293 (1991).
36. C. Homer et al., "Completion of the 2011 National Land Cover Database for the conterminous United States representing a decade of land cover change information," *Photogramm. Eng. Remote Sens.* **81**(5), 346–354 (2015).
37. M. Rutherford, "User guide to displaying GHRSST data using ESRI ArcGIS," Arcgis Help Library. Esri ArcMap 10.2. Redlands, California (2008).
38. T. Blaschke et al., *Object-Based Image Analysis: Spatial Concepts for Knowledge-Driven Remote Sensing Applications*, Springer, Berlin (2008).

39. M. Baatz and A. Schäpe, "Multiresolution segmentation: an optimization approach for high quality multi-scale image segmentation," *Angew. Geogr. Informationsverarbeitung* **12**, 12–23 (2000).
40. L. Yang et al., "A new generation of the United States National Land Cover Database: requirements, research priorities, design, and implementation strategies," *ISPRS J. Photogramm. Remote Sens.* **146**, 108–123 (2018).
41. N. Otsu, "A threshold selection method from gray-level histograms," *IEEE Trans. Syst. Man Cybern.* **9**(1), 62–66 (1979).
42. P. Du et al., "An improved change detection approach using tri-temporal logic-verified change vector analysis," *ISPRS J. Photogramm. Remote Sens.* **161**, 278–293 (2020).
43. I. Fernandez Luque et al., "Non-parametric object-based approaches to carry out ISA classification from Archival Aerial Orthoimages," *IEEE J. Sel. Top. Appl. Earth Obs. Remote Sens.* **6**(4), 2058–2071 (2013).
44. M. Li et al., "A systematic comparison of different object-based classification techniques using high spatial resolution imagery in agricultural environments," *Int. J. Appl. Earth Obs. Geoinf.* **49**, 87–98 (2016).

Rui Guo received her BS degree in geographic information science from Nanjing Normal University, Nanjing, China, in 2019. Currently, she is pursuing her MS degree in cartography and geographical information system at Nanjing University, Nanjing, China. Her research interests include land cover updating and deep learning for remote sensing and land cover change.

Pengfeng Xiao received his BM degree in land resource management from Hunan Normal University, Changsha, China, in 2002 and his PhD in cartography and geographical information system from Nanjing University, Nanjing, China, in 2007. Currently, he is a professor in the Department of Geographic Information Science at Nanjing University. His research interests include high-resolution remote sensing image analysis, remote sensing of snow cover, and land-use and land-cover change.

Xueliang Zhang received his BS degree in geographical information system and his PhD in remote sensing of resources and environment from Nanjing University, Nanjing, China, in 2010 and 2015, respectively. Currently, he is an associate professor in the Department of Geographic Information Science at Nanjing University. His research interests include high-resolution remote sensing image analysis, semantic segmentation, and deep learning for remote sensing.

Hao Liu received his BS degree in geomatics engineering from the Central South University of Forestry and Technology, Changsha, China, in 2017 and his MS degree in photogrammetry and remote sensing from Nanjing University, Nanjing, China, in 2020. He is currently pursuing his PhD in cartography and geographical information system at the same university. His research topics are remote sensing, land cover, and machine learning.